CFD Modeling of Heat Transfer in Turbulent Pipe Flows

S. S. Thakre and J. B. Joshi
Dept. of Chemical Technology, University of Mumbai, Matunga, Mumbai—400019, India

Twelve versions of low Reynolds number k-ϵ and two low Reynolds number Reynolds stress turbulence models for heat transfer were analyzed comparatively. Predictions of the mean axial temperature, the radial and axial turbulent heat fluxes, and the effect of Prandtl number on Nusselt number were compared with the experimental data. The model by Lai and So from the k-ϵ group and Lai and So from the Reynolds stress group had the best overall predictive ability for heat transfer in turbulent pipe flow. The Lai and So model was attributed to its success in the predictions of flow parameters such as mean axial velocity, turbulent kinetic energy, eddy diffusivity, and the overall energy dissipation rate. The k-ϵ models performed relatively better than the Reynolds stress models for predicting the mean axial temperature and the Nusselt number. This qualitative and quantitative study found the need for more sophisticated near-wall experimental measurements and the accuracy of the dissipation (of turbulent energy) and the pressure-scrambling models.

Introduction

In the recent years, low Reynolds number modeling has been widely used for the flow predictions in the turbulent shear flows. The low Reynolds number modeling approach incorporates either a wall-damping effect or a direct effect of molecular viscosity, or both, on the empirical constants and functions in the turbulence transport equations. A fairly complete review of the low Reynolds number k-ϵ modeling of the turbulent shear flows has been given by Patel et al. (1985) and Hrenya et al. (1995). The models reviewed by Patel et al. (1985) and Hrenya et al. (1995) were focused on the flow patterns. Since the heat-transfer process depends entirely on flow pattern, the model that gives good flow predictions can be expected to give good heat transfer predictions as well. However, this statement is in the form of a question. There are few possible reasons for this limitation: (1) there have been rare attempts to extend the flow knowledge from low Reynolds number models to heat transfer; (2) the limitation as regards the accuracy of modeling the energy-dissipation equation (which directly affects the flow quantities and thereby heat transfer); and (3) the difficulty of the turbulent Prandtl number (Pr_t) concept. The Pr_t concept is widely used in an eddy-diffusivity model, in which the eddy diffusivity for momentum is evaluated by either a mixing length model or the k-ϵ model, and the eddy diffusivity for heat is evaluated using Pr_t. The experimental evidence suggests that Pr_t is a number very near unity, and its departure from unity is not great except for very low Prandtl number fluids. However, experimental studies show that the value of Pr_t increases steeply and far exceeds unity as the wall is approached.

There is apparently a possibility of analyzing the behavior of this parameter by using the near-wall turbulent heat-flux models. In one such attempt, Lai and So (1990b) have shown that Pr_t is approximately constant for most of the pipe; however, it increases steeply and far exceeds unity as the wall is approached. Therefore, any heat-transfer model that assumes a constant Pr_t needs very careful analysis, even for simple flows like turbulent pipe flow. However, it must be pointed out that so far no suitable near-wall second moment closure for scalar flux transport has been developed. This is due, in part, to a lack of detailed near-wall scalar flux measurements and partially to the unavailability of an asymptotically correct near-wall Reynolds stress model. Hence, comprehensive work is still needed for the estimation of Pr_t, using turbulent heat-flux models.

Correspondence concerning this article should be addressed to J. B. Joshi.

The shortcomings just cited motivated us to critically analyze the validity of both the low Reynolds number k-ϵ and the Reynolds stress models for the process of heat transfer. The study was restricted to the turbulent pipe flow condition, a relatively simple state, yet of the utmost importance to the chemical engineering community. As a first step, it was thought desirable to critically analyze the existing low Reynolds-number two-equation k-ϵ models and Reynolds stress models for the flow patterns. Numerical codes were developed for more recent versions of twelve low Reynolds number k-ϵ and two low Reynolds number Reynolds stress models for the turbulent pipe flow condition. The knowledge of flow pattern was then used for the numerical prediction of the heat-transfer process. These numerical heat-transfer predictions were compared with the experimental data of Gowen and Smith (1967), Kader (1981), Bremhorst and Bullock (1970, 1973), Hishida et al. (1986), and Mizushina et al. (1971). The present article focuses more on the heat-transfer aspects.

Heat Transfer Analysis from the k-ϵ Models

The low Reynolds number k-ϵ model of turbulence has been widely used in numerical simulations due to its simplicity and, to some extent, capability for predicting wall-bounded turbulent flows. Although these models work well for the flow predictions, they offer some limitations when applied to heat- and mass-transfer calculations at solid boundaries. In these situations they can yield unrealistic predictions for the flux of energy and matter, as well as for the profiles of the corresponding scalar quantities. A literature review shows that the existing near-wall formulations yield reasonable predictions for friction factors and thus for heat-transfer rates when the Prandtl number is of the order of unity, but fail at large Prandtl numbers. At higher Prandtl numbers or at low thermal diffusivity, ν_T values very near the wall have substantial influence on heat-transfer rates.

In view of the shortcomings just cited, it was thought desirable to critically analyze the low Reynolds k-ϵ models for the near-wall heat-transfer predictions. The general computing procedure for heat transfer is to first obtain the flow predictions and then extend this knowledge for the heat-transfer calculations. For this purpose, twelve different low Reynolds number k-ϵ models have been considered. The models selected for the comparison are those of Jones and Launder (1972), Launder and Sharma (1974), Lam and Bremhorst (1981), Chein (1982), Nagano and Tagawa (1988), Myong and Kasagi (1990), Lai and So (1990a), Shih and Mansour (1990), So et al. (1991), Fan et al. (1993), Yang and Shih (1993), and Cho and Goldstein (1994). In the present work, more attention is paid to the heat-transfer aspects. For brevity in the subsequent discussion, these models are referred to as JL, LS, LB, CH, NT, MK, LSO, SM, ST, FLB, YS, and CG model, respectively.

The low Reynolds number model

For steady, isothermal, incompressible, fully developed turbulent pipe flow, the set of governing equations for flow and heat are given as follows.

Flow equations

$$0 = \frac{1}{r}\left[\frac{d}{dr} r\left((\nu + \nu_T)\frac{du}{dr}\right)\right] - \frac{1}{\rho}\left(\frac{dp}{dz}\right)_c, \tag{1}$$

where

$$\nu_T = C_\mu f_\mu \frac{k^2}{\epsilon}. \tag{2}$$

The general form of the transport equations that determine k and ϵ in the low Reynolds number models, simplified for the flows considered here (fully turbulent pipe flow), is given as

$$0 = \frac{1}{r}\left[\frac{d}{dr} r\left(\left(\nu + \frac{\nu_T}{\sigma_k}\right)\frac{dk}{dr}\right)\right] + \nu_T\left(\frac{du}{dr}\right)^2 - \epsilon - D \tag{3}$$

$$0 = \frac{1}{r}\left[\frac{d}{dr} r\left(\left(\nu + \frac{\nu_T}{\sigma_k}\right)\frac{d\epsilon}{dr}\right)\right] + \frac{C_{\epsilon 1} f_1 \nu_T \epsilon}{k}\left(\frac{du}{dr}\right)^2 - \frac{C_{\epsilon 2} f_2 \epsilon^2}{k} + E \tag{4}$$

where C_μ, $C_{\epsilon 1}$, $C_{\epsilon 2}$, σ_k, and σ_ϵ are the same empirical constants found in the standard high Reynolds number k-ϵ models. The functions f_μ, f_1, and f_2, and, in some cases, the D and E terms are included in the low Reynolds number models in order to render the models valid in the near-wall re-

Table 1. Numerical Values for the Constants C_μ, $C_{\epsilon 1}$, $C_{\epsilon 2}$, σ_k, and σ_ϵ for the Low Reynolds Number k-ϵ Models

S. No	Researchers	Model	C_μ	$C_{\epsilon 1}$	$C_{\epsilon 2}$	σ_k	σ_ϵ
1.	Jones and Launder (1972)	JL	0.09	1.45	2.0	1.0	1.3
2.	Launder and Sharma (1974)	LS	0.09	1.44	1.92	1.0	1.3
3.	Lam and Bremhorst (1981)	LB	0.09	1.44	1.92	1.0	1.3
4.	Chein (1982)	CH	0.09	1.35	1.8	1.0	1.3
5.	Nagano and Tagawa (1988)	NT	0.09	1.45	1.9	1.4	1.3
6.	Shih and Mansour (1990)	SM	0.09	1.45	2.0	1.3	1.3
7.	Lai and So (1990a,b)	LSO	0.09	1.35	1.8	1.0	1.3
8.	Myong and Kasagi (1990)	MK	0.09	1.4	1.8	1.4	1.3
9.	So et al. (1991)	SZS	0.096	1.5	1.83	0.75	1.45
10.	Yang and Shih (1993)	YS	0.09	1.44	1.92	1.0	1.3
11.	Fan et al. (1993)	FLB	0.09	1.4	1.8	1.0	1.3
12.	Cho and Goldstein (1994)	CG	0.09	1.44	1.92	1.0	1.3

Table 2. Summary of the Damping Functions f_μ, f_1, and f_2 for the Low Reynolds Number k-ϵ Models

Model	f_μ	f_1	f_2
JL	$\exp[-2.5/(1+R_T/50)]$	1	$1-0.3\exp(-R_T^2)$
LS	$\exp[-3.4/(1+R_T/50)^2]$	1	$1-0.3\exp(-R_T^2)$
LB	$[1-\exp(-0.0165R_y)]^2(1+20.5/R_T)$	$1+(0.05/f_\mu)^3$	$1-\exp(-R_T^2)$
CH	$1-\exp(-0.0115y^+)$	1	$1-(2/9)\exp(-(R_T/6)^2)$
NT	$[1-\exp(-y^+/26.5)^2](1+4.1/R_T^{3/4})$	1	$\{1-0.3\exp[-(R_T/6.5)^2]\}[1-\exp(-y^+/6)]^2$
SM	$1-\exp(-6\times10^{-3}y^+-4\times10^{-4}y^{+2}+2.5\times10^{-6}y^{+3}-4.0\times10^{-9}y^{+4})$	1	$\{1-0.22\exp[-(R_T/6)^2]\}\tilde{\epsilon}/\epsilon$
LSO	$1-\exp(-0.0115y^+)$	$1+\{1-0.6\exp[-\mathrm{Re}/10^4]\}\exp[-(R_T/64)^2]$	$1-(2/9)\exp[-(R_T/6)^2]$
MK	$[1-\exp(-y^+/70)](1+3.45/\sqrt{R_T})$	1	$\{1-(2/9)\exp[-(R_T/6)^2]\}[(1-\exp(-y^+/5)]^2$
SZS	$(1+3.45/\sqrt{R_T})\tanh(y^+/115)$	1	1
YS	$(1+1/\sqrt{R_T})[1-\exp(1.5\times10^{-4}R_y-5.0\times10^{-7}R_y^3-1.0\times10^{-10}R_y^5)]^{1/2}$	$\sqrt{R_T}/(1+\sqrt{R_T})$	$\sqrt{R_T}/(1+\sqrt{R_T})$
FLB	$0.4f_w/\sqrt{R_T}+(1-0.4f_w/\sqrt{R_T})[1-\exp(-R_y/42.63)]^3$ where $f_w=1-\exp\{-\sqrt{R_y}/2.3+(\sqrt{R_y}/2.3-R_y/8.89)[1-\exp(-R_y/20)]^3\}$	1	$\{1-(2/9\exp[-(R_T/6)^2]\}f_w^2$
CG	$1-0.95\exp(-5\times10^{-5}R_T^2)$	1	$1-0.222\exp[-(R_T^2/36)]$

gion. The models vary within the general framework in terms of the assigned constants, damping functions, and the terms D and E as seen from Tables 1, 2, and 3, respectively.

Heat-Balance Equations. The following thermal-energy equation defines the heat-transfer problem:

$$u\frac{\partial T}{\partial x}=\frac{1}{r}\frac{\partial}{\partial r}\left(r\left(\frac{\nu}{Pr}+\frac{\nu_T}{Pr_t}\right)\frac{\partial T}{\partial r}\right). \tag{5}$$

We consider heat transfer in a pipe with constant heat flux through the wall. The convective term on the lefthand side of

Table 3. Summary of the D and E Terms, and Wall Boundary Conditions for k and ϵ for the Low Reynolds Number k-ϵ Models

Model	D	E	Wall Boundary Conditions
JL	$2\nu(d\sqrt{k}/dr)^2$	$2\nu\nu_T(d^2\bar{u}/dr^2)^2$	$k=\epsilon=0$
LS	$2\nu(d\sqrt{k}/dr)^2$	$2\nu\nu_T(d^2\bar{u}/dr^2)^2$	$k=\epsilon=0$
LB	0	0	$k=0;\ \epsilon=\nu d^2k/dr^2$
CH	$2\nu k/y^2$	$(-2\nu\epsilon/y^2)\exp(-0.5y^+)$	$k=\epsilon=0$
NT	0	0	$\frac{\partial k}{\partial y}=0\ \epsilon=y\frac{\partial_k^2}{\partial y^2}$
SM	$2\nu(d\sqrt{k}/dr)^2$	$\nu\nu_T(d^2\bar{u}/dr^2)^2$	$k=0;\ \epsilon=\nu d^2k/dr^2$
LSO	0	$2\nu C_2f_2(\epsilon/k)(d\sqrt{k}/dr)^2+\exp[-(R_T/64)^2]\left(\frac{T}{9}C_2-2\right)\times\epsilon/k(\epsilon-2\nu(d\sqrt{k}/dr))-(1/2k)(\epsilon-2\nu k/y^2)^2)$	$k=0;\ \epsilon=2\nu(d\sqrt{k}/dr)^2$
MK	0	0	$k=0;\ \epsilon=\nu d^2k/dr^2_2$
SZS	0	$2\nu C_2f_2(\epsilon/k)(d\sqrt{k}/dr)^2+\exp[-(R_T/64)^2][-(2\epsilon/k)(\epsilon-2\nu(d\sqrt{k}/dr)^2)+(3/2k)(\epsilon-2\nu k/y^2)^2]$	$k=0;\ \epsilon=\nu\left(\frac{d\sqrt{k}}{dr}\right)$
YS	0	$\nu\nu_T/(d^2\bar{u}/dr^2)^2$	$k=0;\ \epsilon=\nu d^2k/dr^2$
FLB	0	0	$k=0;\ \frac{\partial\epsilon}{\partial r}=0$
CG	0	S_ϵ	$k=0;\ \frac{\partial\epsilon}{\partial r}=0$
	$S_\epsilon=1.44(1-f_\mu)[(2\nu\nu_T(d^2u/dr^2)^2+2\nu(d\sqrt{k}/dr)^2(\epsilon/k))]+\max[0.83(\epsilon^2/k)(l/C_1y-1)(l/C_1y)^2,0.0]$		

Eq. 5 was normalized according to Yakhot et al. (1987). The heat equation (Eq. 5) was normalized as: $r^+ = r/R$; $u^+ = u/u_\tau$; $T^+ = T/T^*$, where $T^* = q/C_P \rho u_\tau$, and $\nu^+ = \nu/u_\tau R$, $\nu_T^+ = \nu_T/u_\tau R$.

Boundary conditions

Since the flow is axisymmetric, only the boundary conditions at the wall and the symmetry line are required to the specified:

$$r = 0; \qquad \frac{du}{dr} = \frac{dk}{dr} = \frac{dT}{dr} = 0$$

$$r = R; \qquad u = k = 0; \qquad q = -\kappa \frac{dT}{dr}. \tag{6}$$

As summarized by Patel et al. (1985), three boundary conditions have been employed in the past for dissipation variable. These are $\epsilon_w = 0.$; $(\partial\epsilon/\partial y)_w = 0$; $\epsilon_w = \nu(\partial^2 k/\partial y^2)_w$ or the equivalent $\epsilon_w = \nu(2k/y^2)_w$. The boundary conditions used by various authors are summarized in Table 3. Equation 5, along with the boundary conditions (Eq. 6), was solved by the numerical technique outlined in the fourth section. Since the heat transfer and the momentum equations present a set of coupled equations, the eddy viscosity and the axial velocity profiles obtained from flow are used for the solution of the thermal energy equation (Eq. 5). Their iterative procedure was implemented for the simulations of the momentum equations to obtain the complete flow details, and these results were used for the solution of the heat equation. Thus, only one iteration was enough for getting the temperature profile. The only input used for solving the heat problem was the Prandtl number. The turbulent Prandtl number was assigned a constant value of $Pr_t = 1$.

Heat-Transfer Analysis from the Turbulent Heat-Flux Models

Although much progress has been achieved in recent years in the modeling of the Reynolds stress transport equations, the modeling of the scalar field, on the other hand, is still rather primitive. This is because, the model development of the heat flux depends largely on the availability and correctness of turbulent stresses predicted by the Reynolds-stress model. Furthermore, heat-flux transport is influenced by more than one time scale. Consequently, it is more difficult to achieve a closure of the heat-flux transport equations than the Reynolds-stress equations. In addition, a shortage of reliable and relatively accurate near-wall heat-flux measurements also contributes to the slow development of a near-wall turbulence model for heat fluxes. Realizing the limitation of the calculation methods based on Pr_t, researchers try to improve the modeling by turning to two equation k-ϵ and the algebraic flux models for heat transport. Despite some success, it is still believed that the most reliable prediction methods are those based on a second moment closure. The reason is that the turbulent interactions that generate the Reynolds stresses and heat fluxes can be treated with less empiricism. A detailed literature review shows that, so far, no suitable near-wall second moment closure for scalar flux transport has been developed. This is due, in part, to a lack of detailed near-wall scalar measurements and, partially, to the unavailability of an asymptotically correct near-wall Reynolds-stress model.

In view of this shortcoming, the model proposed by Lai and So (1990a) looks promising. Lai and So (1990a) (LSO), developed a near-wall Reynolds-stress turbulence model that can correctly predict the anisotropy of the turbulent normal stresses. The success of that model motivated Lai and So (1990b) to extend the momentum approach to model turbulent heat transport near a wall. The modeling approach was similar to that outlined in Lai and So (1990a) and was based on the limiting wall behavior of the heat-flux transport equations. This way, the modeled equation was valid all the way to the wall and the assumption of a temperature wall function, and a constant turbulent Prandtl number was not required. Prud'homme and Elghobashi (1986) (PEL) proposed a second-order closure for momentum and the algebraic stress model for the heat transfer. In the present work, some modifications have been incorporated in the heat-transfer part. The algebraic stress model for heat was replaced with the second moment heat closure of LSO. This modification was mainly due to our interest in the low Reynolds number second moment closures for heat, and to present a comparative study of the predictive capability of these two models for heat transfer.

Model of Lai and So

Flow Equations. Lai and So (1990a) solved the full Reynolds stress closure along with the mean axial velocity and the dissipation rate equation:

$$\nu \frac{du}{dr} - \overline{u'v'} + \frac{ru_\tau^2}{R} = 0 \tag{7}$$

$$\frac{1}{r}\frac{d}{dr}\left[r\left(\nu + C_s \frac{k}{\epsilon}\overline{v^2}\right)\frac{d\overline{u}'^2}{dr}\right] + \frac{1}{r}\frac{d}{dr}\left[rC_s \frac{k}{\epsilon} 2\overline{u'v'}\frac{d\overline{u'v'}}{dr}\right]$$
$$-2\left(1 - \frac{2}{3}\alpha + \frac{1}{3}\beta + \frac{2}{3}\alpha^* f_{w,1}\right)\overline{u'v'}\frac{du}{dr}$$
$$- C_1(1 - f_{w,1})\frac{\epsilon}{k}\left(\overline{u'^2} - \frac{2}{3}k\right) - \frac{2}{3}\epsilon(1 - f_{w,1})$$
$$- f_{w,1}\frac{\epsilon}{k}\frac{\overline{u'^2}}{\left(1 + \frac{3\overline{v'^2}}{2k}\right)} = 0 \tag{8}$$

$$\frac{1}{r}\frac{d}{dr}\left[r\left(\nu + 3C_s \frac{k}{\epsilon}\overline{v'^2}\right)\frac{d\overline{v}'^2}{dr}\right] - \frac{2}{r}C_s \frac{k}{\epsilon}\overline{v'^2}\frac{d\overline{w'^2}}{dr}$$
$$- \frac{4}{r^2}C_s \frac{k}{\epsilon}\overline{w'^2}\left(\overline{v'^2} - \overline{w'^2}\right) + \frac{2\nu}{r^2}\left(\overline{w'^2} - \overline{v'^2}\right)$$
$$- \frac{2}{3}(\alpha - 2\beta - \alpha^* f_{w,1})\overline{u'v'}\frac{du}{dr} - C_1(1 - f_{w,1})\frac{\epsilon}{k}\left(\overline{v'^2} - \frac{2}{3}k\right)$$
$$- \frac{2}{3}\epsilon(1 - f_{w,1}) - 2f_{w,1}\frac{\epsilon}{k}\overline{v'^2} - 4f_{w,1}\frac{\epsilon}{k}\frac{\overline{v'^2}}{\left(1 + \frac{3\overline{v'^2}}{2k}\right)} = 0 \tag{9}$$

Table 4. Numerical Values of Constants for the Low Reynolds Number Reynolds Stress Models

Researchers	Model	C_1	C_2	C_3	$C_{\epsilon 1}$	$C_{\epsilon 2}$	C_s	C_ϵ	α^*	α	β	γ
Prud'homme and Elghobashi (1986)	PEL	1.17	0.3	0.123	1.45	1.9	0.25	0.15		(1/11) $(8+C_2)$	(1/11) $(8C_2-2)$	(1/55) $(30C_2-2)$
Lai and So (1990)	LSO	1.5	0.4	—	1.35	1.8	0.11	0.15	0.45	(1/11) $(8+C_2)$	(1/11) $(8C_2-2)$	(1/55) $(30\ C_2-2)$

$$\frac{1}{r}\frac{d}{dr}\left[r\left(\nu+C_s\frac{k}{\epsilon}\overline{v'^2}\right)\frac{d\overline{w}'^2}{dr}\right]+\frac{2}{r}\frac{d}{dr}\left[C_s\frac{k}{\epsilon}\overline{w'^2}\left(\overline{v'^2}-\overline{w'^2}\right)\right.$$
$$\left.+\frac{4}{r^2}C_s\frac{k}{\epsilon}\overline{w'^2}\left(\overline{v'^2}-\overline{w'^2}\right)\right]+\frac{2}{r}C_s\frac{k}{\epsilon}\overline{v'^2}\frac{d\overline{w'^2}}{dr}$$
$$-\frac{2}{3}(\alpha+\beta-\alpha^* f_{w,1})\overline{u'v'}\frac{du}{dr}$$
$$-C_1(1-f_{w,1})\frac{\epsilon}{k}\left(\overline{w'^2}-\frac{2}{3}k\right)+\frac{2\nu}{r^2}\left(\overline{v'^2}-\overline{w'^2}\right)-\frac{2}{3}\epsilon(1-f_{w,1})$$
$$-f_{w,1}\frac{\epsilon}{k}\frac{\overline{w'^2}}{\left(1+\frac{3\overline{v'^2}}{2k}\right)}=0 \quad (10)$$

$$\frac{1}{r}\frac{d}{dr}\left[r\left(\nu+2C_s\frac{k}{\epsilon}\overline{v}'^2\right)\frac{d\overline{u'v'}}{dr}\right]+\frac{1}{r}\frac{d}{dr}\left[rC_s\frac{k}{\epsilon}\overline{u'v'}\frac{d\overline{v'^2}}{dr}\right]$$
$$-\frac{1}{r}\left[C_s\frac{k}{\epsilon}\overline{u'v'}\frac{d\overline{w'^2}}{dr}+2\frac{\overline{w'^2}}{r}\right]-(1-\alpha+\alpha^* f_{w,1})\overline{v'^2}\frac{du}{dr}$$
$$-\left(\beta\overline{u'^2}-\gamma k\right)\frac{du}{dr}-C_1(1-f_{w,1})\frac{\epsilon}{k}\overline{u'v'}$$
$$-f_{w,1}\frac{\epsilon}{k}\overline{u'v'}-2f_{w,1}\frac{\epsilon}{k}\frac{\overline{u'v'}}{\left(1+\frac{3\overline{v'^2}}{2k}\right)}=0 \quad (11)$$

$$\frac{1}{r}\frac{d}{dr}\left[r\left(\nu+C_\epsilon\frac{k}{\epsilon}\overline{v}'^2\right)\frac{d\bar{\epsilon}}{dr}\right]-C_{\epsilon 1}(1+\sigma f_{w,2})\overline{u'v'}\frac{du}{dr}$$
$$-C_{\epsilon 2}f_\epsilon\frac{\epsilon\bar{\epsilon}}{k}+f_{w,2}\left[\left(\frac{7}{9}C_{\epsilon 2}-2\right)\frac{\epsilon\bar{\epsilon}}{k}-\frac{1}{2}\frac{\epsilon^{*2}}{k}\right]=0. \quad (12)$$

The model constants used in the preceding closures are given in Table 4. The expressions for the damping functions employed in these models are given in Table 5.

Heat-Balance Equations. Lai and So (1990b) solved the full turbulent heat-flux closures along with the mean axial temperature equation:

$$\alpha\frac{1}{r}\frac{\partial}{\partial r}\left(r\frac{\partial T}{\partial r}\right)-\frac{1}{r}\frac{d}{dr}\left(r\overline{v'T'}\right)=u\frac{\partial T}{\partial x}. \quad (13)$$

The heat-flux terms $\overline{v'T}$ and $\overline{u'T'}$ were expressed by the following equations:

$$\frac{1}{r}\frac{d}{dr}\left(r\left(\nu+\frac{\alpha-\nu}{3}+2C_s^\theta\frac{k}{\epsilon}\overline{v'^2}\right)\frac{d\overline{v'T'}}{dr}\right)$$
$$-\frac{2}{r}C_s^\theta\frac{k}{\epsilon}\overline{w'^2}\frac{\overline{v'T'}}{r}-\left(\nu+\frac{\alpha-\nu}{3}\right)\frac{\overline{v'T'}}{r^2}-\overline{v'^2}\frac{\partial T}{\partial r}$$
$$-\overline{u'v'}\frac{\partial T}{\partial x}-(1-f_{w,\theta})C_{1\theta}\frac{\epsilon}{k}\overline{v'T'}-C_{1\theta,w}\frac{\sqrt{k}}{R-r}\overline{v'T'}$$
$$-f_{w,\theta}\frac{\epsilon}{k}\overline{v'T'}-f_{w,\theta}\left(1+\frac{1}{Pr}\right)\frac{\epsilon}{k}\overline{v'T'}=0 \quad (14)$$

$$\frac{1}{r}\frac{d}{dr}\left(r\left(\nu+\frac{\alpha-\nu}{2}+C_s^\theta\frac{k}{\epsilon}\overline{v'^2}\right)\frac{d\overline{u'T'}}{dr}\right)$$
$$+\frac{1}{r}\frac{d}{dr}\left(rC_s^\theta\frac{k}{\epsilon}\overline{u'v'}\frac{d\overline{v'T'}}{dr}\right)-\overline{u'v'}\frac{\partial T}{\partial x}-\overline{u'^2}\frac{\partial T}{\partial x}$$
$$-\overline{v'T'}\frac{du}{dr}-(1-f_{w,\theta})C_{1\theta}\frac{\epsilon}{k}\overline{u'T'}+C_{2\theta,w}\overline{v'T'}\frac{du}{dr}$$
$$-\frac{f_{w,\theta}}{2}\left(1+\frac{1}{Pr}\right)\frac{\epsilon}{k}\overline{u'T'}=0. \quad (15)$$

Table 5. Summary of the Damping Functions and Wall Boundary Conditions for Turbulent Kinetic Energy Dissipation Rate for the Low Reynolds Number Reynolds Stress Models

Model	f_μ	f_{s1}	f_{s2}	$f(s)$	f_{w1}	f_{w2}	f_ϵ	Wall Boundary Conditions
PEL	$\exp[(-3.4)/(1+R_T/50)^2]$	$\left(1+\frac{R_T}{10}\right)^{-1}$	—	—	—	—	$1-(1-(1.4/C_{\epsilon 2}))\exp[-(R_T/36)^2]$	$\frac{\partial\epsilon}{\partial r}=0$
LSO	$1-\exp(0.0115y^4)$	—	—	—	$\exp[-(R_T/150)^2]$	$\exp[-(R_T/64)^2]$	$1-(2/9)\exp[-(R_T/6)^2]$	$\epsilon=2\nu(d\sqrt{k}/dr)^2$

Model of Prud'homme and Elghobashi

Flow Equations. Prud'homme and Elghobashi (1986) solved the full Reynolds-stress closure along with the mean axial velocity and the dissipation rate equation:

$$\nu\frac{du}{dr}-\overline{u'v'}+\frac{ru_\tau^2}{R}=0 \tag{16}$$

$$\frac{1}{r}\frac{d}{dr}\left[r\left(\nu+C_s f_\mu\frac{k}{\epsilon}\overline{v'^2}\right)\frac{d\overline{u'^2}}{dr}\right]-2\left((1-\alpha)+\frac{2}{3}(\alpha+\beta)+\frac{2}{3}f_s\right)\overline{u'v'}\frac{du}{dr}-C_1\frac{\epsilon}{k}\overline{u'^2}+\frac{2}{3}\epsilon(C_1-1)=0 \tag{17}$$

$$\frac{1}{r}\frac{d}{dr}\left[r\left(\nu+C_s f_\mu\frac{k}{\epsilon}\overline{v'^2}\right)\frac{d\overline{v'^2}}{dr}\right]+2\overline{u'v'}\beta\frac{du}{dr}-\frac{2}{3}(\alpha+\gamma)\overline{u'v'}\frac{du}{dr}-C_1\frac{\epsilon}{k}\overline{v'^2}+2C_3\overline{u'v'}\frac{du}{dr}f(s)-2\left[\left(\nu+C_s f_\mu\frac{k}{\epsilon}\overline{w'^2}\right)\frac{\left(\overline{v'^2}-\overline{w'^2}\right)}{r}\right] \tag{18}$$

$$\frac{1}{r}\frac{d}{dr}\left[r\left(\nu+C_s f_\mu\frac{k}{\epsilon}\overline{w'^2}\right)\frac{d\overline{w'^2}}{dr}\right]-\frac{2}{3}(\alpha+\beta)\overline{u'v'}\frac{du}{dr}-C_1\frac{\epsilon}{k}\overline{w'^2}+\frac{2}{3}\epsilon(C_1-1)-2\left[\left(\nu+C_s f_\mu\frac{k}{\epsilon}\overline{w'^2}\right)\frac{\left(\overline{v'^2}-\overline{w'^2}\right)}{r}\right]=0 \tag{19}$$

$$\frac{1}{r}\frac{d}{dr}\left[r\left(\nu+C_s f_\mu\frac{k}{\epsilon}\overline{v'^2}\right)\frac{d\overline{u'v'}}{dr}\right]-\beta_1\frac{du}{dr}+(C_1+f(s))\frac{\epsilon}{k}\overline{u'v'}+\left[\left(\nu+C_s f_\mu\frac{k}{\epsilon}\overline{w'^2}\right)\frac{\overline{u'v'}}{r^2}\right]-C_3\left[\left(\overline{u'^2}-\overline{v'^2}\right)\frac{du}{dr}\right]f(s)=0 \tag{20}$$

$$\frac{1}{r}\frac{d}{dr}\left[r\left(\nu+C_\epsilon f_\mu\frac{k}{\epsilon}\overline{v^2}\right)\frac{d\epsilon}{dr}\right]-C_{\epsilon 1}\frac{\epsilon}{k}\overline{u'v'}\frac{du}{dr}-C_{\epsilon 2}f_\epsilon\frac{\epsilon^2}{k}+C_{\epsilon 2}f_\epsilon\frac{\epsilon}{k}\nu\left(\frac{d\sqrt{k}}{dr}\right)^2+2\nu\frac{k}{\epsilon}f_\mu\overline{v'^2}\left(\frac{d^2u}{dr^2}\right)^2=0. \tag{21}$$

Heat-Balance Equations. Prud'homme and Elghobashi (1986) proposed an algebraic-stress model for the heat transport. In the present work, however, the algebraic-stress model was replaced with the turbulent heat-flux model of Lai and So (1990b) given by Eqs. 13–15.

Boundary conditions

Since the flow is axisymmetric, only the boundary conditions at the wall and the symmetry line are required to be specified. These are

$$u=\overline{u'^2}=\overline{v'^2}=\overline{w'^2}=\overline{u'v'}=0$$

$$\epsilon=2\nu\left(\frac{\partial\sqrt{k}}{\partial y}\right)\qquad\text{at}\qquad r=R$$

$$q=-\kappa\frac{dT}{dr},\qquad\overline{v'T'}=\overline{u'T'}=0\qquad\text{at}\qquad r=R$$

$$\frac{d\epsilon}{dr}=\frac{d\overline{u'^2}}{dr}=\frac{d\overline{v'^2}}{dr}=\frac{d\overline{w'^2}}{dr}=0,\qquad\overline{u'v'}=0\qquad\text{at}\qquad r=0$$

$$\frac{\partial T}{\partial r}=\frac{d\overline{u'T'}}{dr}=0\qquad\overline{v'T'}=0\qquad\text{at}\qquad r=0, \tag{22}$$

The energy-balance analysis over a control volume between x and $x+dx$ and the fully developed condition gives

$$\frac{\partial T}{\partial x}=\frac{2q}{\rho C_p u_b R}. \tag{23}$$

To obtain the solution for the governing equations, first the dependent and independent variables are normalized in the following manner: u by u_τ, $\overline{u_i'u_j'}$ by u_τ^2, ϵ by u_τ^3/R, (T_w-T) by T^*, $\overline{u_i'T'}$ by $u_\tau T^*$, and r by R. The expression for normalized heat-transfer coefficient (Nusselt number) was obtained in the following form:

$$Nu^+=\frac{2\,Re^*Pr}{T^+}. \tag{24}$$

This equation was used for the numerical predictions of Nusselt numbers from both the k-ϵ and Reynolds-stress models.

Method of Solution

The solution procedure consisted of two steps: the first step was to solve the momentum equations to obtain the mean axial velocity, the normal stresses, the Reynolds stresses, the turbulent kinetic energy (k), and the turbulent kinetic energy dissipation rate (ϵ). Since the momentum and heat-flux equations present a set of coupled equations, the flow information obtained from step one was used in step two: to obtain the mean temperature and turbulent heat-flux distributions. Thus, the solution for the coupled momentum–heat model necessitates the solution of four ordinary differential equations for k-ϵ models and nine for the Reynolds-stress models. The governing equations for both, the k-ϵ models as well as Reynolds-stress closures, are ordinary differential equations, and therefore can be solved by any iteration scheme for split boundary-value problems. The dependent variables were normalized by u_τ and u_τ/R (u by u_τ, k by u_τ^2, and ϵ by u_τ^3/R), while the r coordinate was normalized by R so that the integration was carried out from symmetry line to the wall. Thus formulated, $Re=u_\tau R/\nu=(u_\tau/2u_0)R_D$ became the only input parameter to the fully developed flow calculations, where $R_D=u_0 2R/\nu$, and u_0 is the mean axial

velocity at the pipe center. Similarly, for heat transfer, Pr was the only input parameter needed to be defined.

A finite-volume technique proposed by Patankar (1980) was used for the solution of the four coupled nonlinear ordinary differential equations for k-ϵ models and nine equations for Reynolds-stress models. The integration was carried from center to the wall. In all the cases, a nonuniform grid was used to carry out the calculations. Grid generation is one of the important aspects of the numerical simulation. The robustness of any numerical code depends on the effectiveness and stability of the grid-generation scheme employed for investigation. In the present work, the following two grid-generation techniques were employed:

1. By locating more than half of the points in the range $r/R \geq 0.9$. This method gave good predictions for both k-ϵ and Reynolds-stress closures. However, it was observed that for high Reynolds number, it shows inefficiency to depict the peak in the turbulence quantities. Moreover, for high grid densities (above 120 grid points), as should be used for higher Reynolds number and Prandtl number flows, this method leads to the numerical error.

2. By obtaining an increasingly fine mesh as the wall is approached. This grid system was found to be most effective for both the k-ϵ and Reynolds-stress closures. Moreover, this method worked fine for high grid densities (up to 180 grid points), and hence was useful at higher Reynolds number and Prandtl number flows.

The first technique was found to be useful only for the LB model. For the remaining models, the second technique was preferred due to the reasons just cited. The predictions obtained from both techniques (1) and (2) were found to be insensitive to the grids, since doubling the number of grid points changed the solution profiles by less than 1%. Although the influence of grid density on flow is expected, the degree of sensitivity is more for heat transfer. This is especially true for the case of higher Prandtl number, the reason being that, at higher Prandtl numbers, the thickness of the thermal boundary becomes smaller than the viscous sublayer. Hence, the heat transfer gets confined to a very small region near the wall. In order to effectively capture the steep temperature gradients in this region, it is essential to define fine grid size in the near wall region. In the present work, the grid densities used ranged from 70 to 120 points. The number and concentration of grid points used depended on the Reynolds and Prandtl numbers under consideration.

Results and Discussions

Comparison of numerical predictions with the experimental data for k-ϵ models

In order to validate the low Reynolds number k-ϵ models for heat transfer, the fully developed pipe flow temperature measurements with constant wall heat-flux boundary conditions were chosen. Unlike the measurements of flow quantities, such as the mean velocity and Reynolds stresses, the accurate experimental data on the temperature profiles are scarce. Moreover, there are very few cases where measurements are reported for higher Prandtl numbers. The few important experimental investigations in this regard are those of Johnk and Hanratty (1962) for $Pr = 0.72$; Gowen and Smith (1967) for $Pr = 5.7$ and 14.3; Slarciauskas et al. (1973) for $Pr = 64.0$; and Kader (1981) for $Pr = 95$ and 170. In the present investigation, the low Prandtl number data ($Pr = 5.7$) of Gowen and Smith (1967) and high Prandtl number data (Pr

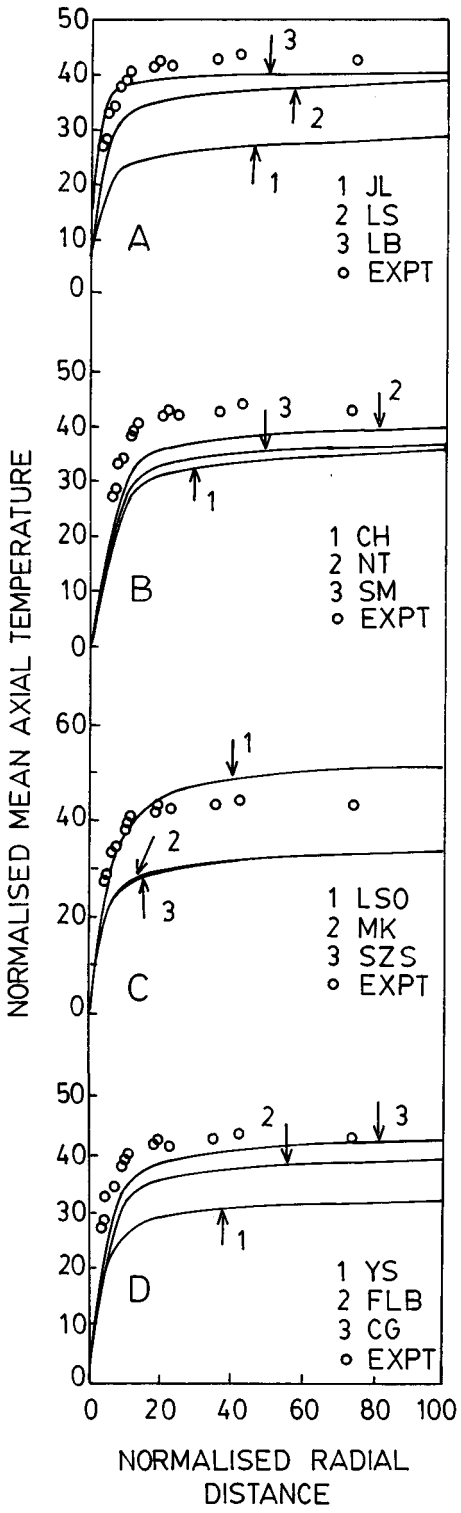

Figure 1. Comparison of the mean axial temperature predictions of k-ϵ models with the experimental data of Gowen and Smith (1967) for Prandtl number = 5.7.

= 95 and 170) of Kader (1981) have been used to test the validity of the models.

The predictions of mean axial temperature profiles for $Pr = 5.7$ are compared with the experimental data of Gowen and Smith (1967) in Figure 1. It can be noted that the temperatures were normalized with respect to the heat flow rate, heat capacity, and friction velocity, so that the Reynolds number independence is attained. It can be observed from Figure 1 that only the LB, LSO, and CG models agree fairly well with the experimental data. Most of the models were found to underpredict the experimental data. The comparison was relatively better for the LSO model over the whole range of the experimental data.

The predictions for $Pr = 95$ and 170 have been validated with the experimental data of Kader (1981). The results are shown in Figure 2. Figure 2a shows the comparison for JL, LS, and LB models. It can be observed that none of these models compare well with the experimental data. The JL model underpredicts, while the LS and LB models overpredict, the experimental data. Of the three, the LS model compares fairly well with the experimental data. Figure 5 indicates that the underpredictions of the JL model and the overpredictions of the LS model may be due to the higher k profiles of the former and the lower of the latter. However, both the models, in accordance with the experimental data, were able to depict the location where the profiles change slope. The profile of the LB model was quite unrealistic in the sense that it neither gave the proper location of the change of slope (the location was observed to be close to the wall), nor did it give the proper wall value (the wall value was 300 for LB, as compared to 80 for JL and LS). This may be due to the improper damping functions used, leading to the inaccurate predictions of ν_T and/or the turbulent kinetic energy dissipation rate in the near-wall region. The predictions of the dissipation variable (ϵ) in the near wall region reflects on the eddy viscosity profiles. Hence, any model that fails to correctly predict ϵ in the near-wall region, will lead to inaccurate ν_T, and consequently the temperature predictions. The temperature predictions obtained from CH, NT, and SM are given in Figure 2b. The CH model underpredicts the experimental data, while NT and SM compare well with the experimental data. The SM model slightly underpredicts the experimental data. The comparison of the LSO, MK, and SZS models is given in Figure 2c. The LSO model slightly overpredicts the experimental data toward the central region; otherwise, the comparison is good. Both the MK and SZS models give values that are too low compared to the experimental data. The comparison of the YS, FLB, and CG models is given in Figure 2d. It can be observed that CG is in good agreement with the experimental data, while FLB and YS underpredict the experimental profile. The reasons for the observed discrepancies in various models may be the same as explained for Figure 2a.

The comparison for $Pr = 170$ is given in Figure 3. In this case, the experimental data by Kader (1981) are available in the near-wall zone. The comparison for $Pr = 170$ sets a crucial test for the validation of the models for temperature, because of the very small thermal boundary-layer thickness. The temperature profiles from various models have been compared in Figures 3a–3d. The trend observed for JL, LS, and LB in Figure 3a was similar to Figure 2a. Here, too, the JL model underpredicted and LS overpredicted the experimental data, while the LB model predictions were quite unrealistic. In Figure 3b the SM and NT models were in better agree-

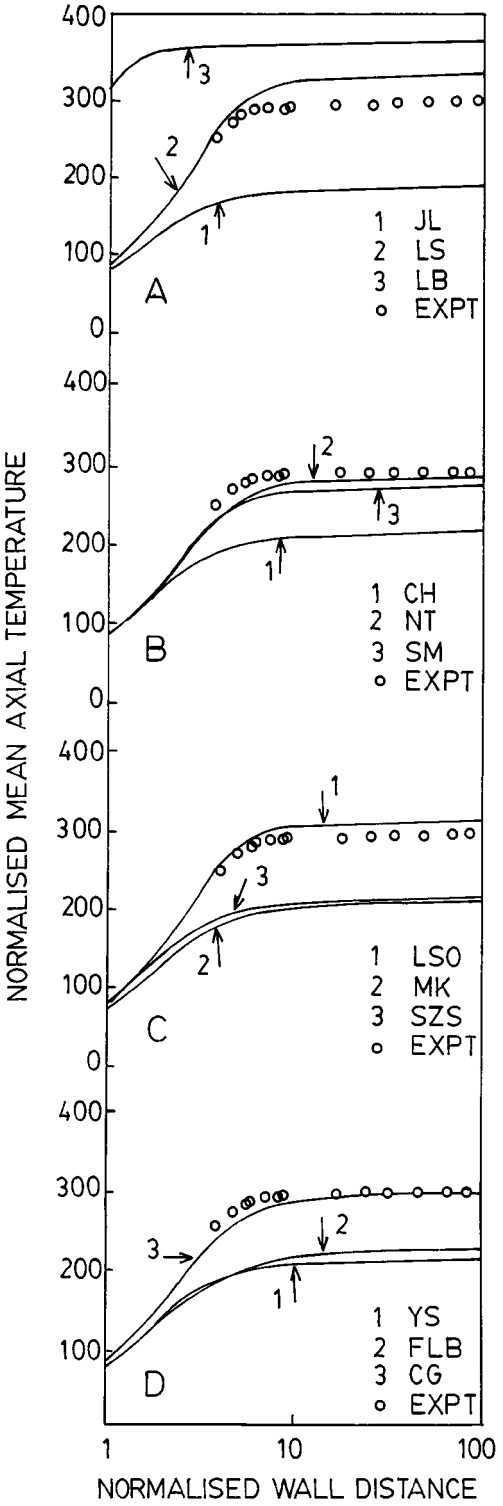

Figure 2. Comparison of the mean axial temperature predictions of k-ϵ models with the experimental data of Kader (1981) for Prandtl number = 95.

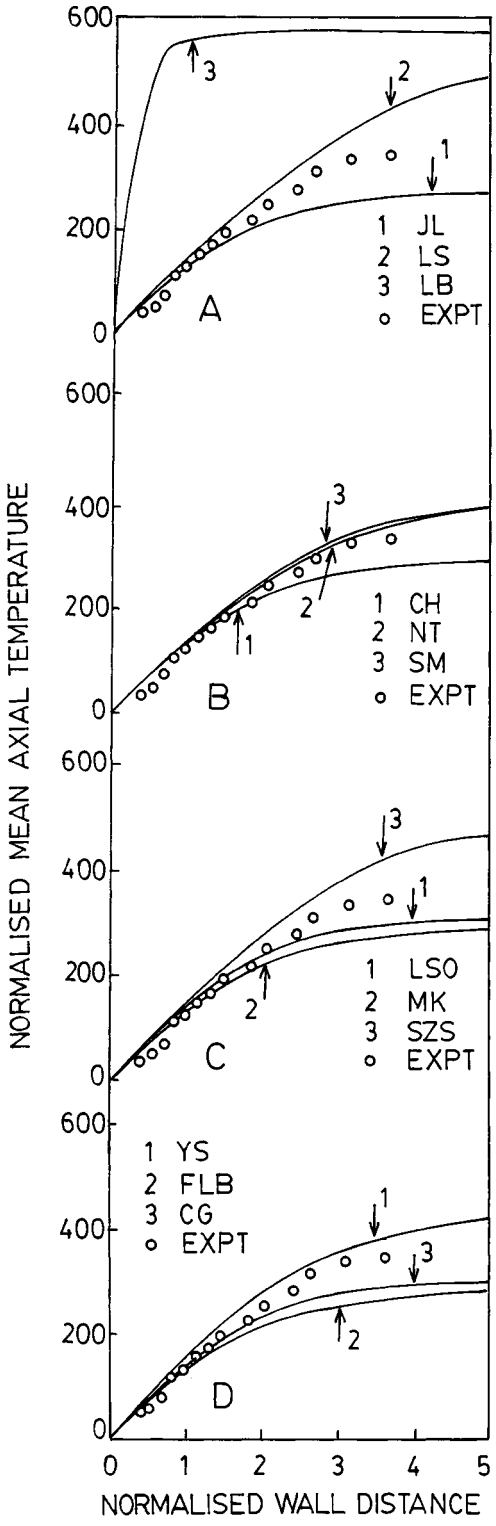

Figure 3. Comparison of the mean axial temperature predictions of k-ϵ models with the experimental data of Kader (1981) for Prandtl number = 170.

ment with the experimental data, while the CH model underpredicted. Once again, the results obtained were similar to Figure 2b. From Figures 3c and 3d, the LSO and CG models were found to be in good agreement with the experimental data. In spite of these discrepancies, most of the models were found to be in good agreement with the experimental data for $y^+ \leq 2$.

From the comparison study of Figures 1, 2, and 3, it can be observed that the LSO model is in overall good agreement with the experimental data for either of the three Prandtl numbers. The remaining models faired poorly for either of the three Prandtl numbers. Since the LSO model compares well, it was thought desirable to analyze the relative performance of these models for the predictions of flow parameters such as axial velocity, turbulence kinetic energy, and eddy diffusivity. For the first two parameters, the experimental data of Durst et al. (1995) was used. For eddy diffusivity, the experimental data of Schildknecht et al. (1979) was used. Since the near-wall region is of importance for the prediction of temperature profiles, attention has been focused on this region, particularly for comparison of the k and ν_T profiles. The results are given in Figures 4, 5, and 6, respectively. From Figure 4 it can be seen that the JL, CH, NT, SM, LSO, MK, SZS, and YS models show very good agreement with the experimental data of mean axial velocity ($0 < y^+ < 200$). Practically all the models (except LS) are able to predict the k profiles (Figure 5) in the y^+ range of 0 to 100. For eddy diffusivity (Figure 6), fairly good predictions are made by the JL, LS, LSO, and MK models.

It was also thought that it was desirable to establish overall energy balance. The total (viscous and turbulent) energy dissipation rate can be calculated by the following equation:

$$\epsilon_{\text{expt}} = \frac{\Delta P \times \text{Vol.flow rate}}{\text{Volume of the pipe}}. \tag{25}$$

Normalizing the above equation (ϵ by u_τ^3/R and u by u_τ), we get

$$\epsilon^+_{\text{expt}} = fu^{+3}. \tag{26}$$

The predicted energy dissipation rate consists of viscous and turbulent energy dissipation rates:

$$\epsilon^+_{\text{predicted}} = \epsilon^+_{\text{turbulent}} + \epsilon^+_{\text{mean}}, \tag{27}$$

where

$$\epsilon^+_{\text{mean}} = \nu^+ \overline{\left(\frac{\partial u^+}{\partial r^+}\right)^2} \tag{28}$$

$$\epsilon_{\text{turbulent}} = \nu \overline{\frac{\partial u_i'}{\partial x_j}\frac{\partial u_i'}{\partial x_j}}. \tag{29}$$

The comparison between the experimental and the predicted dissipation rates is presented in Table 6. It can be seen that the LSO, CG, and FLB models predict the energy dissipation rate within 4%. The difference is large for the other models.

From the foregoing discussion it is clear that the LSO model is the best if we consider the predictive ability for all

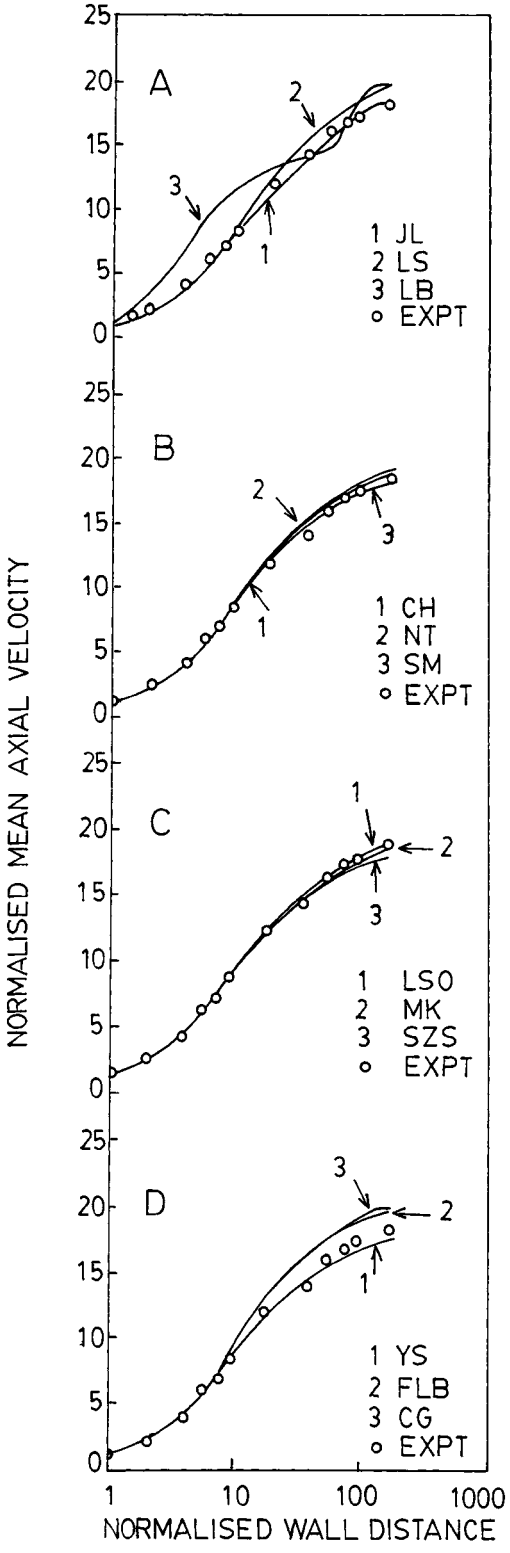

Figure 4. Comparison of the mean axial velocity predictions of the k-ϵ model with the experimental data of Durst et al. (1995) for Reynolds number = 7442.

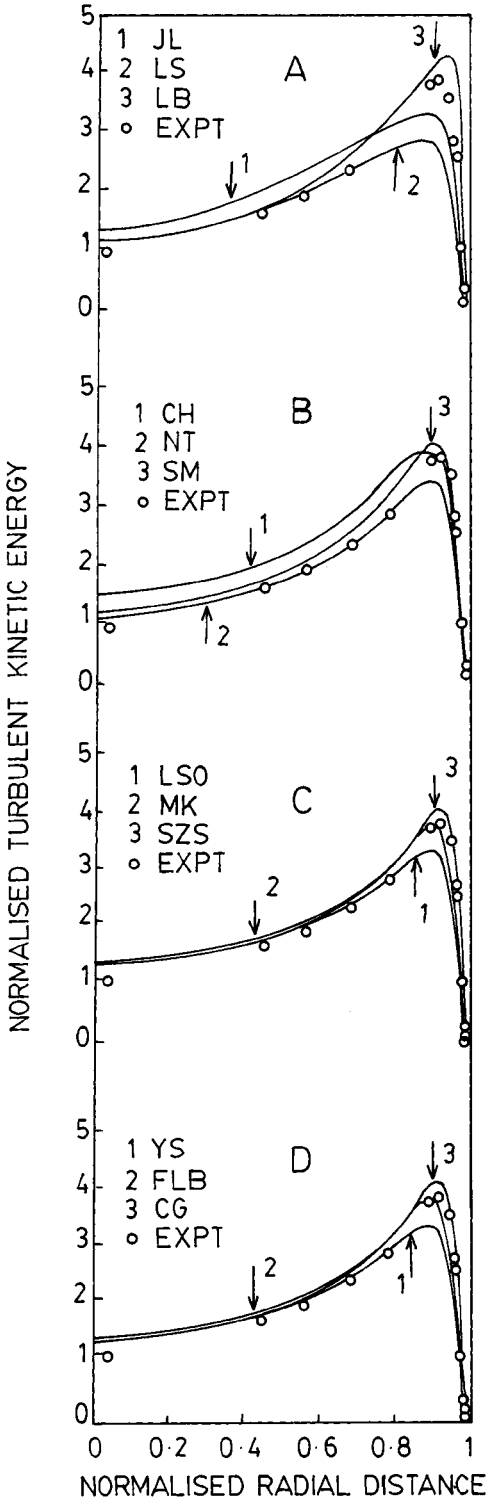

Figure 5. Comparison of the turbulent kinetic energy predictions of the k-ϵ model with the experimental data of Durst et al. (1995) for Reynolds number = 7442.

four parameters u, k, ν_T, and the energy balance. This ability of the LSO model probably explains its success in the prediction of temperature profiles, as shown in Figures 1 to 3.

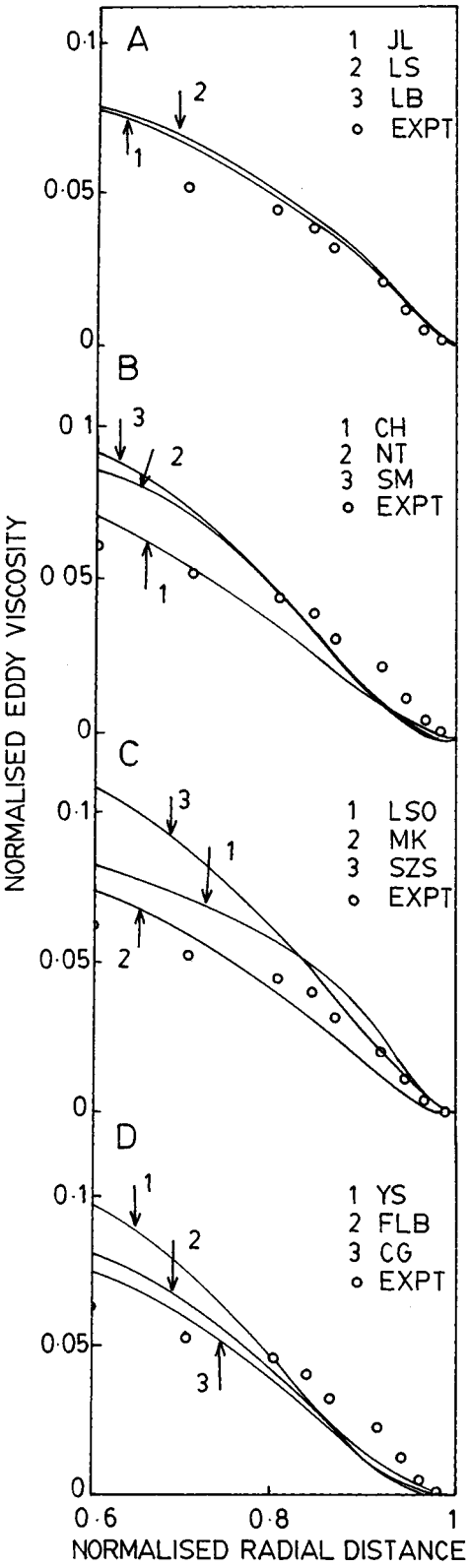

Figure 6. Comparison of the eddy viscosity predictions of the k-ϵ model with the experimental data of Schildknecht (1979) for Reynolds number = 22,000.

Table 6. Numerical Simulation and the Energy Balance Calculations for $Re = 22{,}000$

Model	No. of Grid Points Required (Range)	Convergence Criteria	No. of Iterations Required (Range)	Energy Input (Eq. 26)	Total ϵ^+ (Eq. 27)
JL	75–85	10^{-4}–10^{-5}	100–200	35.61	29.90
LS	75–85	10^{-4}–10^{-5}	100–200	35.61	32.47
LB	75–85	10^{-4}–10^{-5}	100–200	35.61	33.14
CH	75–85	10^{-4}–10^{-5}	100–200	35.61	31.42
NT	75–85	10^{-4}–10^{-5}	150–250	35.61	33.26
SM	75–85	10^{-4}–10^{-5}	200–300	35.61	31.63
LSO	75–85	10^{-4}–10^{-5}	150–250	35.61	34.39
MK	75–85	10^{-4}–10^{-5}	150–250	35.61	33.25
SZS	75–85	10^{-4}–10^{-5}	100–200	35.61	30.84
YS	75–85	10^{-4}–10^{-5}	150–250	35.61	32.26
FLB	75–85	10^{-4}–10^{-5}	100–200	35.61	34.94
CG	75–85	10^{-4}–10^{-5}	200–250	35.61	34.94

Although the LSO model has been shown to be the best, additional work is still needed for closure predictions. It is known that, in addition to eddy diffusivity, there are other factors that can contribute to the poor predictions. These are the assumption of the constant turbulent Prandtl number and the near-wall measurement limitations. In the present investigation, the turbulent Prandtl number was assigned a constant value of 1.0. If a constant turbulent Prandtl number is assumed, the entire thermal field depends only on eddy diffusivity. In fact, some previous experimental evidence suggests that the turbulent Prandtl number does not remain constant; rather, it takes a value higher than unity very near the wall. Second, the discrepancy observed between the numericla predictions and experimental data may be due to the uncertainity of the data caused by the experimental difficulties involved in measurements close to the wall, which are needed at high Prandtl numbers.

Comparison of numerical predictions with the experimental data for Reynolds-stress models

In order to validate the near-wall turbulent heat-flux models of Prud'homme and Elghobashi (1986) and Lai and So (1990b), the data of Gowen and Smith (1967) and Kader (1981), Bremhorst and Bullock (1970, 1973), and Hishida et al. (1986) were used for checking the predictive capability of models as regards to the mean axial temperature, the normal and axial heat fluxes, and for the calculation of the Nusselt number. The comparison for the normal and axial turbulent heat fluxes is hindered due to the scarcity and the reliability of the experimental data. In this respect, the preceding experimental measurements were found to be reasonably accurate for the comparison. The calculations were carried out to assess the correctness and validity of the near-wall heat-flux closure as regards its ability to predict the mean temperature profiles, the normal, and axial turbulent heat fluxes.

LSO compared their mean temperature profiles with the experimental data of Johnk and Hanratty (1962) for very low Prandtl number of $Pr = 0.7$. The predictions of mean temperature profiles were obtained for two cases: in the presence as well as in the absence of the wall reflection term. This was done to quantify the effect of this term on the tem-

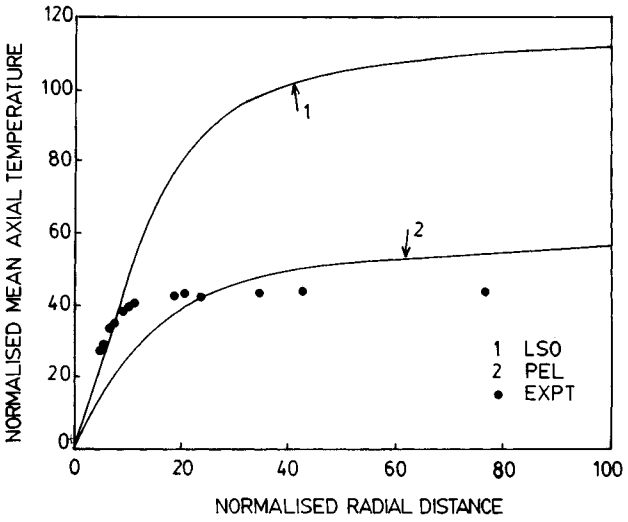

Figure 7. Comparison of the mean axial temperature predictions of Reynolds stress models with the experimental data of Gowen and Smith (1967) for Prandtl number = 5.7.

perature profiles. In the present case, however, the predictions were obtained with the consideration of the wall reflection terms. Figure 7 shows the comparison for $Pr = 5.7$, while Figures 8 and 9 give the comparison for $Pr = 95$ and $Pr = 170$, respectively. It can be seen from these figures, that none of the models compare over the whole range of experimental data. For $Pr = 5.7$ and 95, it was observed that, the predictions from the LSO model agree well with the experimental data up to $y^+ \prec 8$; however, a steep increase up to $y^+ = 15$ was observed. The predictions from the PEL model were appreciably lower than the experimental data in the near-wall region ($y^+ \prec 10$). It can be seen from Figure 8, that for $y^+ \succ 100$, the predictions from both models gave an irregular pattern. The irregularity in LSO arose at a lower y^+ as compared to the PEL model. It is believed that the discrepancy is due to the incorrect high Reynolds-number modeling of the pressure-scrambling and diffusion terms. In Figure 9, the predictions from LSO model were once again fairly good compared to the PEL model. This analysis indicates that the LSO model is in the best overall agreement with the experimental data for the Prandtl numbers under consideration.

The comparisons of the calculated and measured heat fluxes are shown in Figures 10 and 11. Comparison of the predicted turbulent axial heat flux with the experimental data of Bremhorst and Bullock (1970, 1973) is given in Figure 10, while comparison of predicted turbulent radial heat flux with the experimental data of Hishida et al. (1986) is given in Figure 11. For streamwise turbulent heat flux ($\overline{u'T'}$), it was observed that both models overpredict the experimental data. The discrepancy was large near the wall, since the difference in the peak values of predicted and experimental data was observed to be higher at that point. According to LSO (1990b), the discrepancy between the model predictions and experiments could be attributed to measurement errors generated by flow distortion due to buoyancy, and also partly to the simple one-time scale model of pressure scrambling. Shih and Lumley (1986) argued that the pressure-scrambling process is influenced by more than one time scale and proceeded to propose modifications to the pressure-scrambling model. The preceding reasons justify the discrepancy observed between the predictions and the experimental data for the estimation of streamwise turbulent heat flux, and implies the need for more sophisticated models so that the present approach can again be used to derive an asymptotically correct near-wall turbulent heat-flux model.

The radial turbulent heat-flux comparison is given in Figure 11. The accurate estimation of this variable is crucial since it is the controlling factor for the mean temperature and streamwise turbulent heat-flux calculations. It can be seen that the LSO model compares well with the experimental data in the near wall region up to $y^+ \prec 12$. However, for $y^+ \succ 15$, predictions start deviating, and there is a sudden flatness in the curve in the region $12 \prec y^+ \prec$ center of the column. Indeed, the flatness is observed in the experimental curve, too, but it occurs at larger values of the normalized wall distance, $y^+ \succ 25$. The predictions from the PEL model disagreed with

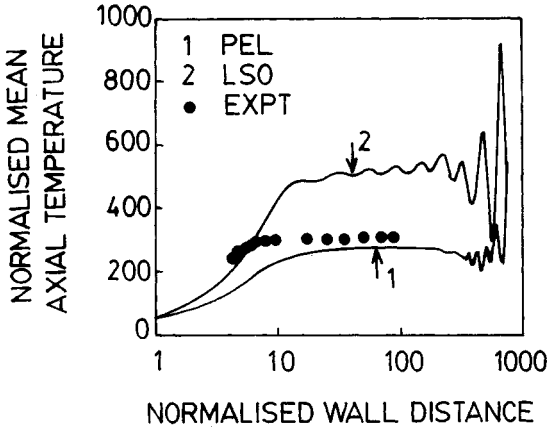

Figure 8. Comparison of the mean axial temperature predictions of Reynolds stress models with the experimental data of Kader (1981) for Prandtl number = 95.

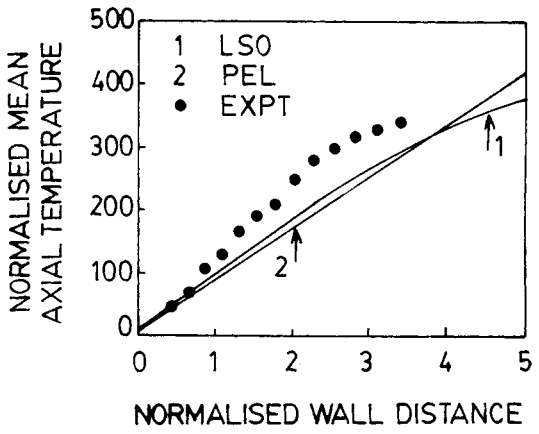

Figure 9. Comparison of the mean axial temperature predictions of Reynolds stress models with the experimental data of Kader (1981) for Prandtl number = 170.

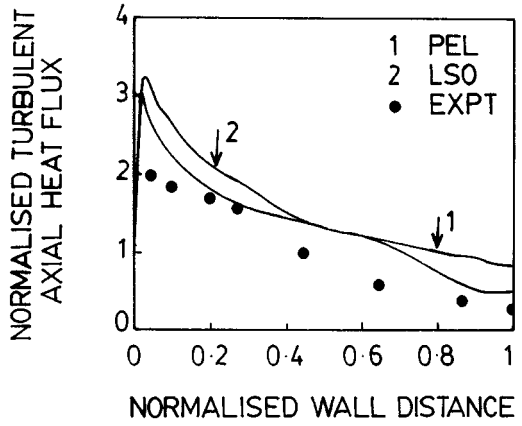

Figure 10. Comparison of the turbulent axial heat-flux predictions with the experimental data of Bremhorst and Bullock (1970, 1973).

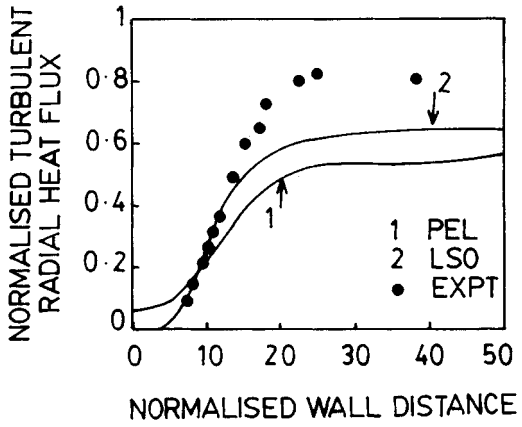

Figure 11. Comparison of the turbulent radial heat flux predictions with the experimental data of Hishida et al. (1986).

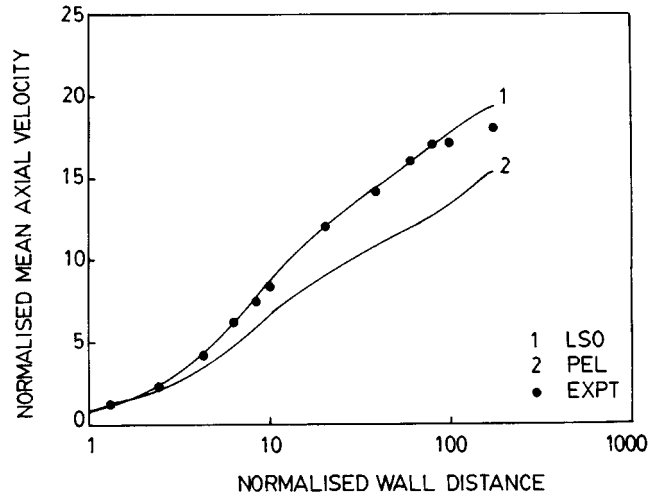

Figure 12. Comparison of the mean axial velocity predictions of the Reynolds stress models with the experimental data of Durst et al. (1995) for Reynolds number = 7442.

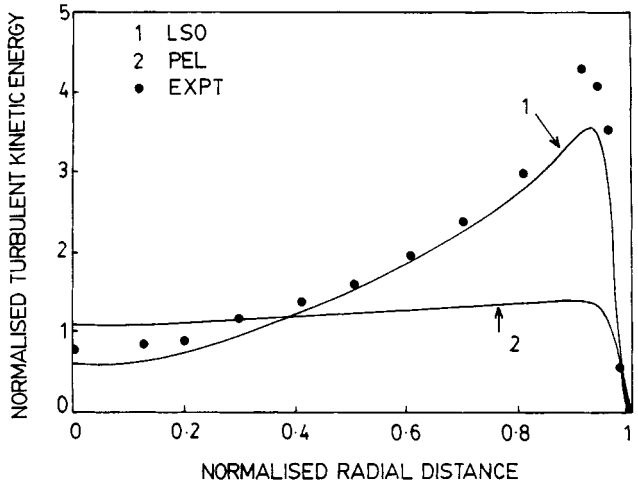

Figure 13. Comparison of the turbulent kinetic energy predictions of the Reynolds stress models with the experimental data of Durst et al. (1995) for Reynolds number = 7442.

the experimental data both near the wall and toward the center. Near the wall, the predictions were higher, while a substantial decrease was observed toward the center. The accurate prediction of $\overline{v'T'}$ near the wall region from LSO is reflected in the mean temperature predictions as seen from Figures 7, 8, and 9. It can be seen that the good prediction of this quantity (obtained by LSO) compares well with the mean axial temperature.

Similar to the k-ϵ model, the success of the LSO model under the RSM category can also be explained on the basis of its ability to predict the flow parameters such as mean axial velocity (u), turbulent kinetic energy (k), and the radial rms fluctuating velocity. The results are shown in Figures 12, 13, and 14, respectively. It can be seen that the predictions of the LSO model are very close to the experimental data.

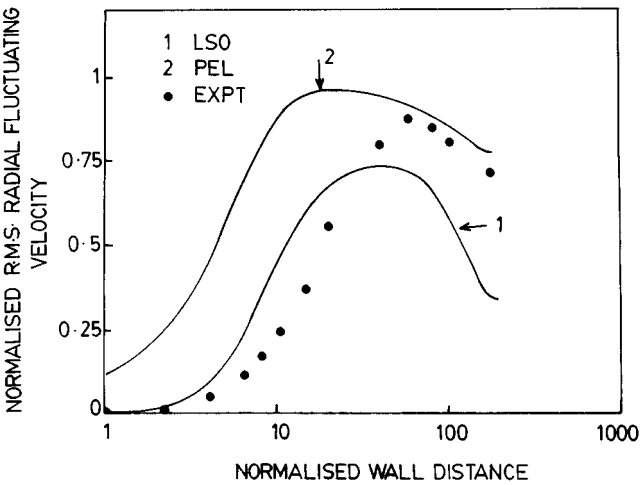

Figure 14. Comparison of the rms radial velocity component predicted by Reynolds stress models with the experimental data of Durst et al. (1995) for Reynolds number = 7442.

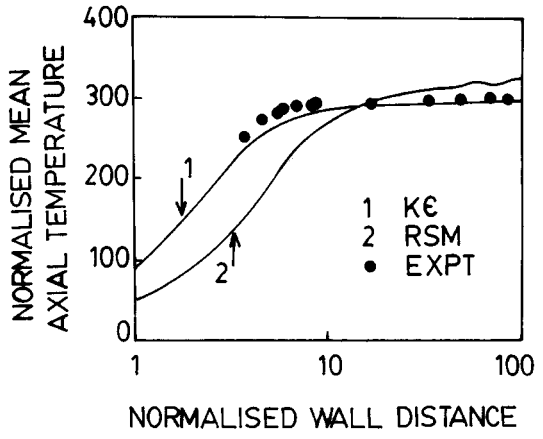

Figure 15. Comparison of the mean axial temperature predictions of the k-ϵ and the Reynolds stress models with the experimental data of Kader (1981) for Prandtl number = 170.

Comparison of the k-ϵ and Reynolds-stress models for heat transfer

The mean temperature profiles obtained from the k-ϵ and the Reynolds-stress models are compared in Figure 15. For this study, the NT model from the $k-\epsilon$ group and the LSO model from the RSM group were selected. It can be seen that the overall comparison is better for the k-ϵ model. The second comparison was sought for the predictive capability of the k-ϵ and RSM models for the heat-transfer coefficients. The predicted Nu vs. Pr profile was compared with the experimental data of Mizushina et al. (1971). The comparison is given in Figure 16. It can be seen from Figure 16 that the NT model compares well with the experimental data up to $Pr \leq 100$. At higher Prandt numbers, however, the model slightly underpredicted the experimental data. On the other hand, comparison of the LSO (Reynolds-stress model) model was poor for the whole range of Prandtl numbers.

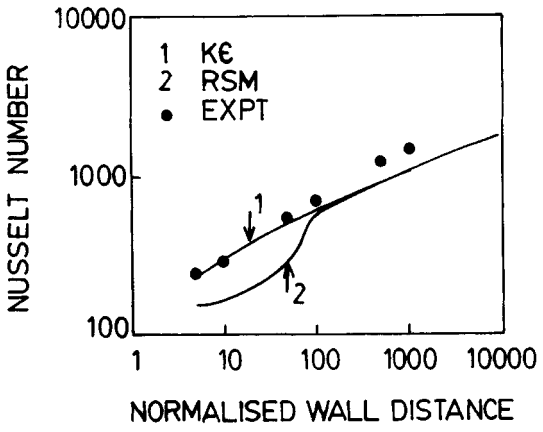

Figure 16. Comparison of the Nusselt number predictions of the k-ϵ and the Reynolds stress models with the experimental data of Mizushina et al. (1971).

Conclusions

The heat-transfer analysis presented in this study shows that the LSO model of the k-ϵ and Reynolds-stress groups were in overall good agreement with experimental data for the three Prandtl numbers. The disagreement for the axial heat flux ($\overline{u'T'}$) predictions was due to one time scale model of pressure scrambling. The comparative analysis between the k-ϵ and RSM models for the mean temperature and the Nusselt number predictions favor the applicability of the $k-\epsilon$ model for heat transfer. Even though the RSM model overcomes the assumptions of isotropy and the constancy of turbulent Prandtl number, its applicability to heat transfer is suspected. This is mainly due to the speculation that the heat-flux transport is more complicated than momentum transport, and is more likely to be influenced by two or more time scales than by one. The second reason may be due to the inappropriate near-wall modeling of the dissipation and the pressure-scrambling terms. The predictive ability of the k-ϵ models is expected to improve when the Pr_t variation near the wall is included. Further, the overall discrepancy observed in both the k-ϵ and the RSM models for heat transfer can be attributed to the incorrect near-wall modeling of the dissipation term and the lack of detailed near-wall temperature and scalar flux measurements at higher Prandtl numbers.

Notation

C_P = specific heat at constant pressure, kJ·kg^{-1}·°C^{-1}
C_1 = constant in the k-ϵ and Reynolds-stress models
$C_{1\theta}, C_{2\theta}$ = constants used in turbulent heat-flux model
$C_{1\theta,w}, C_s^{\theta}$ = constants used in turbulent heat-flux model
D = term contained in the k equation
$(dp/dz)_c$ = constant axial pressure gradient
E = term contained in the ϵ equation
f = friction factor
f_μ, f_1, f_2 = damping functions used in low Reynolds number k-ϵ and Reynolds-stress models
$f_\epsilon, f_{w,1}$ = damping functions used in low Reynolds number Reynolds-stress models
$f_{w,\theta}$ = damping function used in low Reynolds number turbulent heat-flux model
k = turbulent kinetic energy, m^2·s^{-2}
k^+ = normalized turbulent kinetic energy (k/u_τ^2)
P = pressure, N·m^{-2}
p' = fluctuating pressure, N·m^{-2}
q = constant wall heat flux, W·m^{-2}
q_{eff} = effective radial heat flux, [$=(k+\rho C_p \epsilon_H)\partial T/\partial y$], W·m^{-2}
R = radius of pipe, m
R_D = normalized radius of pipe, ($2Ru_0/\nu$)
R_T = turbulent Reynolds number ($k^2/\nu\epsilon$)
R_y = turbulent Reynolds number based on y ($k^{1/2}y/\nu$)
Re = Reynolds number based on mean velocity ($2Ru/\nu$)
Re^* = Reynolds number based on friction velocity (Ru_τ/ν)
Sc = Schmidt number
St = Stanton number
T = mean axial temperature, °C
T_w = mean axial temperature at the wall, °C
T^* = temperature based on friction velocity ($= q/C_p\rho u_\tau$), °C
T^+ = normalized mean axial temperature (T/T^*)
u = mean axial fluid velocity, m·s^{-1}
u_b = bulk mean axial velocity of fluid, m·s^{-1}
u_τ = friction velocity [$=\sqrt{-R(dp/dz)_c/(2\rho)}$]
u' = fluctuating axial fluid velocity, m·s^{-1}
u^+ = normalized mean axial fluid velocity (u/u_τ)

$\overline{u'T'}^+$ = normalized turbulent axial heat flux ($=\overline{u'T'}/u_\tau T^*$)
$\overline{v'T'}^+$ = turbulent radial heat flux ($=\overline{v'T'}/u_\tau T^*$)
v = mean radial fluid velocity, $m \cdot s^{-1}$
v' = fluctuating radial velocity component, $m \cdot s^{-1}$
w = mean tangential fluid velocity, $m \cdot s^{-1}$
w' = fluctuating tangential velocity component, $m \cdot s^{-1}$
y = normal distance from wall ($R - r$)
y^+ = dimensionless wall distance (yu_τ/ν)
z = axial coordinate

Greek letters

$\alpha, \alpha^*, \beta, \gamma$ = constants in low Reynolds number Reynolds-stress model
κ = thermal conductivity, $W \cdot m^{-1} \cdot °C^{-1}$
μ = molecular viscosity of fluid, $kg \cdot m^{-1} \cdot s^{-1}$
μ_t = turbulent viscosity of fluid, $kg \cdot m^{-1} \cdot s^{-1}$
ρ = density of fluid, $kg \cdot m^{-3}$
ν = molecular kinematic viscosity of liquid, $m^2 \cdot s^{-1}$
ν_T = turbulent kinematic viscosity or eddy diffusivity, $m^2 \cdot s^{-1}$
σ = surface tension, $N \cdot m^{-1}$
σ_k = turbulent Prandtl number for k
σ_ϵ = turbulent Prandtl number for ϵ
ϵ = turbulent kientic energy dissipation rate, $m^2 \cdot s^{-3}$
ϵ^+ = normalized turbulent kinetic energy dissipation rate ($\epsilon R/u_\tau^3$)
$\tilde{\epsilon}$ = pseudodissipation variable ($\epsilon - D$)
ϵ_H = eddy diffusivity for heat, $m^2 \cdot s^{-1}$
ΔP = pressure drop, $N \cdot m^{-2}$

Literature Cited

Bremhorst, K., and K. J. Bullock, "Spectral Measurements of Temperature and Longitudinal Velocity Fluctuations in Fully Developed Pipe Flow," *Int. J. Heat Mass Transfer*, **13**, 1313 (1970).

Bremhorst, K., and K. J. Bullock, "Spectral Measurements of Turbulent Heat Transfer in Fully Developed Pipe Flow," *Int. J. Heat Mass Transfer*, **16**, 2141 (1973).

Chein, K. V., "Prediction of Channel and Boundary Layer Flows with a Low Reynolds Number Turbulence Model," *AIAA J.*, **20**, 33 (1982).

Cho, H. H., and R. J. Goldstein, "An Improved Low Reynolds Number $k-\epsilon$ Turbulence Model for Recirculating Flows," *Int. J. Heat Mass Transfer*, **37**, 1495 (1994).

Durst, F., J. Jovonavic, and J. Sender, "LDA Measurements in the Near Wall Region of Turbulent Pipe Flow," *J. Fluid Mech.*, **295**, 305 (1995).

Fan, S., B. Lakshminarayan, and M. Barnett, "Low Reynolds Number $k-\epsilon$ Model for Unsteady Turbulent Boundary Flows," *AIAA J.*, **31**, 1777 (1993).

Gowen, R. A., and J. W. Smith, "The Effect of the Prandtl Number on Temperature Profiles for Heat Transfer in Turbulent Pipe Flow," *Chem. Eng. Sci.*, **22**, 1701 (1967).

Hishida, M., Y. Nagano, and M. Tagawa, "Transport Processes of Heat and Momentum in the Wall Region of Turbulent Pipe Flow," *Proc. Int. Heat Transfer Conf.*, Vol. 3, C. L. Tien et al., eds., Hemisphere, Washington, DC, p. 925 (1986).

Hrenya, C. M., E. J. Boilo, D. Chakrabarti, and J. L. Sinclair, "Comparison of Low Reynolds Number $k-\epsilon$ Turbulence Model in Predicting Fully Developed Pipe Flow," *Chem. Eng. Sci.*, **12**, 1923 (1995).

Johnk, R. E., and T. J. Hanratty, "Temperature Profiles for Turbulent Flow of Air in a Pipe," *Chem. Eng. Sci.*, **17**, 881 (1962).

Jones, W. P., and B. E. Launder, "The Prediction of Laminarization with a Two Equation Model of Turbulence," *Int. J. Heat Mass Transfer*, **15**, 301 (1972).

Kader, B. A., "Temperature and Concentration Profiles in Fully Turbulent Boundary Layers," *Int. J. Heat Mass Transfer*, **24**, 154 (1981).

Lai, Y. G., and R. M. C. So, "On Near Wall Turbulent Flow Modeling," *J. Fluid Mech.*, **221**, 641 (1990a).

Lai, Y. G., and R. M. C. So, "Near Wall Modeling of Turbulent Heat Fluxes," *Int. J. Heat Mass Transfer*, **33**, 1429 (1990b).

Lam, C. K. G., and K. Bremhorst, "A Modified Form of the $k-\epsilon$ Model for Predicting Wall Turbulence," *J. Fluids Eng.*, **103**, 456 (1981).

Launder, B. E., and B. I. Sharma, "Application of Energy Dissipation Model of Turbulence to the Calculation of Flow Near a Spinning Disc," *Lett. Heat Mass Transfer*, **1**, 131 (1974).

Miszushina, T., F. Ogino, Y. Oka, and H. Fukuda, "Turbulence Heat and Mass Transfer Between Wall and Fluid Streams of Large Prandtl and Schmidt Numbers," *Int. J. Heat Mass Transfer*, **14**, 1705 (1971).

Myong, H. K., and N. Kasagi, "A New Approach to the Improvement of $k-\epsilon$ Turbulence Model for Wall Bounded Shear Flows," *JSME Int. J.*, **33**, 63 (1990).

Nagano, Y., and M. Tagava, "A Improved $k-\epsilon$ Model for Boundary Layer Flows," *J. Fluids Eng.*, **112**, 33 (1988).

Patankar, S. V., *Numerical Heat Transfer and Fluid Flow*, McGraw-Hill, New York (1980).

Patel, V. C., W. Rodi, and G. Scheuerer, "Turbulence Models for Near Wall and Low Reynolds Number Flows: A Review," *AIAA J.*, **23**, 1308 (1985).

Prud'homme, M., and S. Elghobashi, "Turbulent Heat Transfer Near the Reattachment of Flow Downstream of a Sudden Pipe Expansion," *Numer. Heat Transfer*, **10**, 349 (1986).

Schildknecht, M., J. A. Miller, and G. E. A. Meier, "The Influence of Suction on the Structure of Turbulence in Fully Turbulent Pipe Flow," *J. Fluid Mech.*, **90**, 67 (1979).

Shih, T. H., and J. L. Lumley, "Influence of Time Scale Ratio on Scalar Heat Flux Relaxation; Modelling Sirivat and Warhaft's Homogeneous Passive Scalar Fluctuations," *J. Fluid Mech.*, **162**, 211, (1986).

Shih, T. H., and N. N. Mansour, "Modelling of Near Wall Turbulence," *Engineering Turbulence Modeling and Experiments*, Elsevier, Amsterdam (1990).

Slarciauskas, A. A., A. A. Pedisius, and A. A. Zukauskas, "Universal Profiles of the Temperature and Turbulent Prandtl Number in the Boundary Layer on a Plate in a Stream of Fluid," *Tr. Akad. Nauk Lit. SSR*, Ser. B, 2 (1971) (Eng. Transl.: *Heat Transfer Sov. Res.*, **5**, 623 (1973).)

So, R. M. C., H. S. Zhang, and C. G. Speziale, "Near Wall Modelling of the Dissipation Rate Equation," *AIAA J.*, **29**, 2069 (1991).

Yakhot, V., S. A. Orszag, and A. Yakhot, "Heat Transfer in Turbulent Fluids–1. Pipe Flow," *Int. J. Heat Mass Transfer*, **30**, 15 (1987).

Yang, Z., and T. H. Shih, "New Time Scale Based $k-\epsilon$ Model for Near Wall Turbulence," *AIAA J.*, **31**, 1191 (1993).

Manuscript received May 24, 1999, and revision received Mar. 14, 2000.